

Article

An Online State of Charge Estimation Algorithm for Lithium-Ion Batteries Using an Improved Adaptive Cubature Kalman Filter

Zhibing Zeng, Jindong Tian, Dong Li and Yong Tian *

College of Optoelectronic Engineering, Shenzhen University, Shenzhen 518060, China; zengzhibing1994@163.com (Z.Z.); jindt@szu.edu.cn (J.T.); lidong@szu.edu.cn (D.L.)

* Correspondence: ytian@szu.edu.cn; Tel.: +86-755-2690-3761

Received: 17 November 2017; Accepted: 25 December 2017; Published: 1 January 2018

Abstract: An accurate state of charge (SOC) estimation of the on-board lithium-ion battery is of paramount importance for the efficient and reliable operation of electric vehicles (EVs). Aiming to improve the accuracy and reliability of battery SOC estimation, an improved adaptive Cubature Kalman filter (ACKF) is proposed in this paper. The battery model parameters are online identified with the forgetting factor recursive least squares (FRLS) algorithm so that the accuracy of SOC estimation can be further improved. The proposed method is evaluated by two driving cycles, i.e., the New European Driving Cycle (NEDC) and the Federal Urban Driving Schedule (FUDS), and compared with the existing unscented Kalman filter (UKF) and standard CKF algorithms to verify its superiority. The experimental results reveal that comparing with the UKF and standard CKF, the improved ACKF algorithm has a faster convergence rate to different initial SOC errors with higher estimation accuracy. The root mean square error of SOC estimation without initial SOC error is less than 0.5% under both the NEDC and FUDS cycles.

Keywords: state of charge; adaptive cubature Kalman filter; lithium-ion battery; battery model

1. Introduction

With the issues related to industrial development and environmental pollution, electric vehicles have been rapidly developed and promoted in recent years as an environmentally friendly mode of transportation. The lithium-ion battery's features include high energy density, a long lifetime, and a low self-discharge rate, and it accordingly has been widely utilized to be the energy storage system of plug-in hybrid electric vehicles (PHEVs) and pure electric vehicles (PEVs). However, its lifetime feature is well-known to be affected by many factors, such as charge/discharge current, temperature, unbalance in battery cells, depth of charge/discharge, damage evolution caused by the interaction of electrochemical and mechanical phenomena, and the cyclic charge/discharge process [1–7]. Therefore, in order to prolong the battery's lifetime as well as to ensure the battery operates reliability and safety, battery management systems (BMS) have to be developed to monitor and control the whole operating process of lithium-ion batteries [8]. As an indicator of the battery's remaining capacity, the state of charge (SOC) is one of the most critical parameters needed to be accurately predicted. Nevertheless, as an essentially implicit state of the battery, the SOC cannot be directly measured by sensors. Additionally, it is influenced by different types of battery materials and operating conditions [9,10]. Therefore, SOC estimation has been widely studied and many algorithms have been developed to acquire precise SOC values. According to whether a battery model is needed to be established, these SOC estimation methodologies can be roughly categorized as non-model-based methods and model-based methods.

The non-model based methods typically include the look-up table method, the Ampere-hour integral or Coulomb counting method [11,12], the open-circuit voltage method [13], the electrochemical impedance spectroscopy method [14], and machine learning based methods (e.g., artificial neural networks [15,16], fuzzy logic models, and support vector machines [17,18]). For example, Dang et al. [15] investigated open-circuit voltage-based SOC estimation by using a dual neural network fusion battery model. Antón et al. [17] studied the usage of a support vector machine in lithium-ion battery SOC estimation. Li et al. [19] combined a 12-input-2-level merged fuzzy neural network with a reduced-form generic algorithm to predict battery SOC. These non-model-based methods are featured with open-loop estimators, so they have several shortcomings. Firstly, they are incapable of correcting errors caused by factors regardless of inaccurate initial SOC values, measurement noises, or model uncertainties. Secondly, a large number of training data covering all of the driving conditions is required in order to improve the estimation accuracy of the machine learning-based methods, otherwise a large prediction error will be caused by the uncertainty of the new data set. However, it is a huge challenge and time-consuming to collect the large amount of training data needed. Compared with the non-model-based methods, the model-based filtering estimation approaches featured with closed-loop estimators can online correct estimating deviation caused by initial SOC errors, measurement noises, and parameter uncertainties.

Among the model-based methods, the Kalman filter (KF)-based SOC estimation methods have the merits of self-correction, online computation, and the availability of dynamic SOC estimation. They have accordingly been widely studied and commonly used in online SOC estimation. The Kalman filter was originally proposed to estimate the state of linear systems. Later, in order to introduce the KF estimator into nonlinear systems, the extended Kalman filter (EKF) and the unscented Kalman filter (UKF) were developed. The EKF-based and UKF-based methods for battery SOC estimation have been investigated in [20–40], respectively. However, some intrinsic shortcomings of the EKF limit its application in practice. For instance, large errors are possibly caused by the linearizing process of the highly nonlinear battery system. Furthermore, computation of the Jacobian matrix is complicated and may lead to filter instability. Compared with the EKF, the UKF can reduce the estimation error and does not need to calculate the complicated Jacobian matrix. Nevertheless, the EKF and UKF algorithms are both subject to divergence or the curse of dimensionality or both [41]. Later, the cubature Kalman filter (CKF), which is suitable for state estimation of high-order nonlinear systems, was proposed on the basis of the radial-spherical cubature rule [42,43]. In the CKF algorithm, a set of $2n$ points (where n represents the state-vector dimension) is employed to simulate the mean and covariance of states of nonlinear systems suffering from additive Gaussian noise. The process noise covariance and measurement noise covariance are well-known to have a distinct influence on the filtering performance and stability of the KF algorithms. In standard EKF, UKF, and CKF, both the process noise covariance and measurement noise covariance are considered to be constant and their values need to be pre-specified by a trial-and-error process which is time-consuming, laborious, and error-prone. Additionally, for battery SOC estimation, inappropriate values of the noise covariance are very likely to result in a large estimation error. Therefore, an adaptive cubature Kalman filter (ACKF) was presented in [44] to improve the SOC estimation accuracy through the voltage residual-based updating law. However, the converged root mean square error (RMSE) of SOC estimation wildly fluctuates with different initial SOC errors. In addition, the battery model parameters are determined by an offline identification method. In fact, however, the battery parameters are changeable during the discharge or charge process. It is accordingly essential to identify the battery model parameters online.

Aiming to improve the SOC estimation accuracy, in this paper, an adaptive cubature Kalman filter is presented based on the improved Sage–Husa estimator. The values of the process noise covariance matrix and the measurement noise covariance matrix are both adaptively updated according to the output voltage residual sequence of the battery model. Besides, the process noise variance matrix and the measurement noise variance matrix can be ensured to always be non-negative, qualitative, and symmetric, preventing deviation of the SOC estimation results. To establish an accurate battery

model, which is of benefit to further improve the accuracy of SOC estimation, the forgetting factor recursive least squares (FRLS) algorithm is applied to update the battery model parameters online. Experiments based on the New European Driving Cycle (NEDC) and Federal Urban Driving Schedule (FUDS) cycles are carried out for the assessment of the performance of SOC estimation algorithms. In addition, the proposed method is compared with the traditional CKF and UKF algorithms in terms of estimation accuracy and convergence rate to different initial SOC errors.

The remainder of the paper is organized as follows: In Section 2, the battery state space equation based on the Thevenin equivalent circuit model is derived in detail, and the online identification of the battery model parameters using the forgetting factor recursive least squares method is introduced. Section 3 presents the principle of the ACKF-based SOC estimation algorithm. The SOC estimation results are presented and discussed in Section 4, and Section 5 draws the conclusions of the paper.

2. Battery Model and Online Parameters Estimation

2.1. State of Charge Definition

The expression of SOC must be firstly determined before estimating its value. This study uses the traditional definition of the battery SOC, which is defined to be the ratio between the remaining capacity and the nominal capacity formulated as:

$$SOC(t) = SOC(t_0) - \frac{1}{C_n} \int_0^t \eta_c I_L(\tau) d\tau \quad (1)$$

where $SOC(t_0)$ and $SOC(t)$ are separately the SOC at time t_0 and t , C_n is the nominal capacity of the battery, $I_L(\tau)$ is the battery current, which is assumed to be positive in the discharging process but negative in the charging process herein, and η_c is the Coulombic efficiency, which is ignored in this paper.

2.2. Battery Equivalent Circuit Model

A Kalman filter is a kind of algorithm which estimates the system state based on state-space equations, and its estimated results are highly dependent on the system model's accuracy. Thus, an accurate battery model is needed to be established to estimate the SOC based on the Kalman filters. On the other hand, the battery model to be used for online SOC estimation should not be too complicated to reduce the computation cost of the embedded hardware. Therefore, equivalent circuit models (ECMs) are widely used in battery SOC estimation since they have the merits of simplicity and easy online implementation. The equivalent circuit model is a combination of a voltage source, resistors, and capacitors, in which the battery dynamic voltage behaviors are characterized with the resistor–capacitor (RC) ladders. The model is more accurate with more RC ladders, but more complicated. In this paper, the Thevenin model with one RC parallel network is applied due to its good balance between high model accuracy and low implementation complexity. Figure 1 shows the Schematic of the selected Thevenin model.

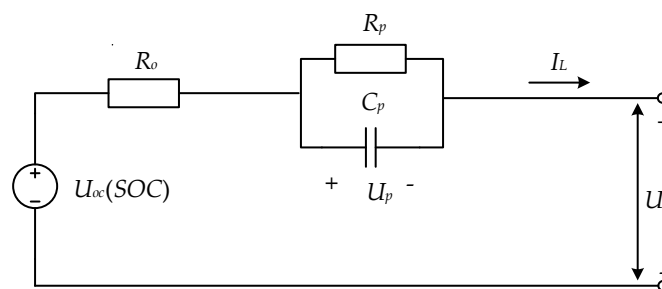


Figure 1. Schematic of the Thevenin model of a lithium-ion battery. SOC: state of charge.

In Figure 1, U_{oc} represents battery open-circuit voltage (OCV), R_o stands for ohmic resistor, R_p is the polarization resistor, C_p is the polarization capacitor, U_t is the battery terminal voltage, and I_L indicates the load current considered to be positive in the discharge process and negative in the charge process.

Based on the Thevenin battery model shown in Figure 1, it can be derived that:

$$\begin{cases} \dot{SOC} = -\frac{1}{C_n} I_L + w_1 \\ \dot{U}_p = -\frac{1}{R_p C_p} U_p + \frac{1}{C_p} I_L + w_2 \end{cases} \quad (2)$$

$$U_t = U_{oc}(SOC) - U_p - R_o I_L + v \quad (3)$$

where the black dots above variables represent the differential operators, U_p is the terminal voltage of C_p , w_1 and w_2 are the process noises added in the SOC and U_p , respectively, for indicating model uncertainties, and v represents the measurement noise added in U_t for indicating the measurement uncertainties. The process noises w_i ($i = 1, 2$) and the measurement noise v are usually assumed to be uncorrelated zero-mean Gaussian white sequences.

Assuming x ($=[SOC, U_p]^T$) as the state vector, I_L as the input variable, and U_t as the output variable, Equations (2) and (3) can be transformed into discrete-time state expressions as:

$$\begin{pmatrix} SOC_k \\ U_{p,k} \end{pmatrix} = \begin{pmatrix} 1 & 0 \\ 0 & \exp(-1/(R_p C_p)) \end{pmatrix} \begin{pmatrix} SOC_{k-1} \\ U_{p,k-1} \end{pmatrix} + \begin{pmatrix} \eta_c/C_n \\ R_p(1 - \exp(-1/(R_p C_p))) \end{pmatrix} I_{L,k-1} + \begin{pmatrix} w_{1,k} \\ w_{2,k} \end{pmatrix} \quad (4)$$

$$U_{t,k} = \left(\frac{dU_{oc}(SOC)}{d(SOC)} \quad -1 \right) \begin{pmatrix} SOC_{k-1} \\ U_{p,k-1} \end{pmatrix} - R_o I_{L,k} + v_k \quad (5)$$

where the subscript k represents the value of the corresponding variable at time step k .

2.3. Online Estimation for Model Parameters

The battery parameters are well-known to be changeable with some factors, e.g., the operating current, depth of charge/discharge, the cyclic charge/discharge process, and temperature, so that a fixed-parameter battery model inevitably leads to significant model error, reducing the SOC estimation accuracy. Therefore, in this study, we use the recursive least squares algorithm with an interactively selected forgetting factor to online identify the battery model parameters for the purpose of improving the battery model accuracy. It will be proved that the online parameter identification-based battery model is valuable for raising SOC estimation accuracy in Section 4.2.

The transfer function of the battery model in Figure 1 can be written as:

$$G(s) = \frac{U_d(s)}{I_L(s)} = \frac{R_p}{1 + R_p C_p s} + R_o \quad (6)$$

where U_d ($=U_{oc} - U_t$) is defined as subtracting the battery terminal voltage U_t from the open-circuit voltage U_{oc} .

Using the bilinear transform rule, i.e., $s = \frac{2}{T} \frac{1-z^{-1}}{1+z^{-1}}$, where T is the sampling period, selected to be one second herein, the discrete-time form of the system transfer function in Equation (6) can be obtained as:

$$G(z^{-1}) = \frac{U_d(z^{-1})}{I_L(z^{-1})} = \frac{k_2 + k_3 z^{-1}}{1 + k_1 z^{-1}} \quad (7)$$

where

$$\begin{aligned} k_1 &= \frac{1-2\tau_p}{1+2\tau_p} \\ k_2 &= \frac{R_o+R_p+2R_o\tau_p}{1+2\tau_p} \\ k_3 &= \frac{R_o+R_p-2R_o\tau_p}{1+2\tau_p} \end{aligned} \quad (8)$$

where $\tau_p = R_p C_p$ is the time-constant of the parallel RC network.

The discrete transfer function in Equation (7) can be further transformed into a time-domain difference equation as:

$$U_{oc}(k) - U_t(k) = -k_1 U_{oc}(k-1) + k_1 U_t(k-1) + k_2 I_L(k) + k_3 I_L(k-1) \quad (9)$$

Define

$$\begin{cases} \varphi(k) = [-(U_{oc}(k-1) - U_t(k-1)); I_L(k); I_L(k-1)] \\ \theta(k) = [k_1; k_2; k_3] \\ y(k) = U_d(k) = U_{oc}(k) - U_t(k) \end{cases} \quad (10)$$

The discrete time-domain difference expression in Equation (9) can be rewritten as:

$$y(k) = \varphi^T(k)\theta(k) + \zeta(k) \quad (11)$$

where ζ is a Gaussian stochastic random noise variable with mean 0.

The vector $\theta(k)$ in Equation (11) can be further solved using the recursive least square algorithm with forgetting factor λ (typically $\lambda = [0.95, 1]$) formulated as:

$$\begin{cases} e(k) = y(k) - \varphi^T(k)\hat{\theta}(k-1) \\ G(k) = \frac{P(k)\varphi(k)}{\lambda + \varphi^T(k)P(k-1)\varphi(k)} \\ \hat{\theta}(k) = \hat{\theta}(k-1) + G(k)e(k) \\ P(k) = \frac{1}{\lambda}(P(k-1) - G(k)\varphi^T(k)P(k-1)) \end{cases} \quad (12)$$

where $e(k)$ is the estimation error of the battery terminal voltage, $G(k)$ is the algorithm gain, and $P(k)$ is the covariance matrix.

Finally, according to the expressions of k_1 , k_2 , and k_3 in Equation (8), the battery model parameters involving R_o , R_p , and C_p can be calculated as:

$$\begin{cases} R_o = \frac{k_2 - k_3}{1 - k_1} \\ R_p = \frac{2(k_3 - k_1 k_2)}{1 - k_1^2} \\ C_p = \frac{(1 - k_1)^2}{4(k_3 - k_1 k_2)} \end{cases} \quad (13)$$

2.4. Battery Model Validation

In Equation (9), the open-circuit voltage U_{oc} is taken as a given parameter, so in order to recursively update the battery model parameters through Equation (13), we need to determine the OCV-SOC equation first. In this study, a sequence of pulsed discharging experiments were implemented for the purpose of collecting the data used to determine the battery OCV-SOC curve. Based on the tested data, a fifth-order polynomial in Equation (14) is selected to characterize the dynamic variation of OCV with SOC, and the measured data and fitted curve are simultaneously presented in Figure 2. It can be seen

that the fitted curve nearly goes across each tested data point, revealing that the selected fifth-order polynomial can characterize the variation of OCV with SOC very well.

$$OCV = 10.5592 \times SOC^5 - 32.1144 \times SOC^4 + 36.3038 \times SOC^3 - 18.5391 \times SOC^2 + 4.913764.91376 \times SOC + 3.0253 \quad (14)$$

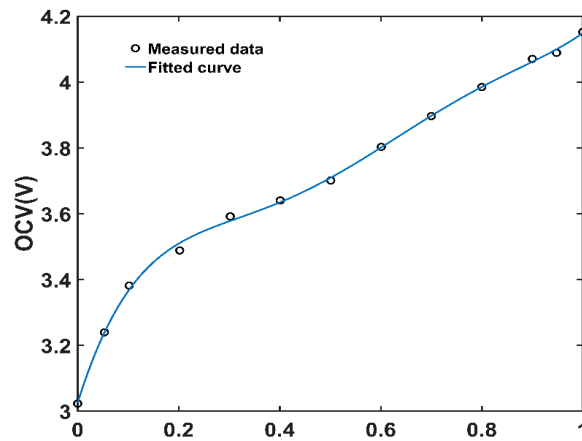


Figure 2. Variation of OCV with SOC.

In this study, the estimated battery terminal voltage is compared with the measured one to assess the accuracy of the online parameter determination. Results based on the New European Driving Cycle (NEDC) and Federal Urban Driving Schedule (FUDS) tests are shown in Figures 3a and 4a, respectively, and the associated voltage errors are presented in Figures 3b and 4b. From Figure 4, it is clear that the relative maximum error and mean error under the NEDC are, respectively, about 0.69% and 0.0286%, and those under the FUDS are about 1.55% and 0.0358%, respectively. Therefore, we can conclude that the variable parameter battery model with online parameter update can well-simulate the dynamic voltage behaviors of the battery.

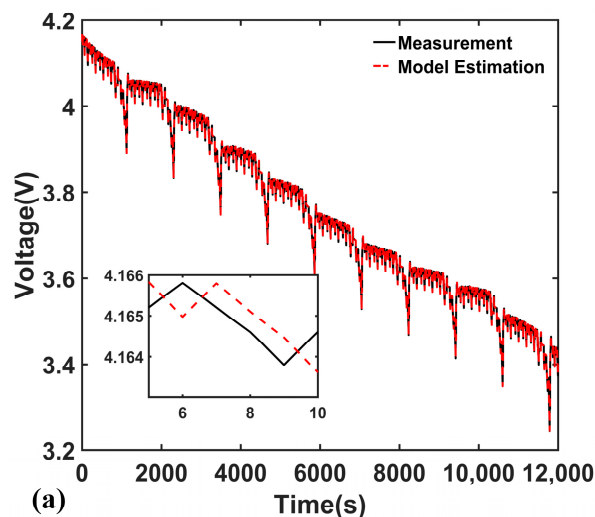


Figure 3. Cont.

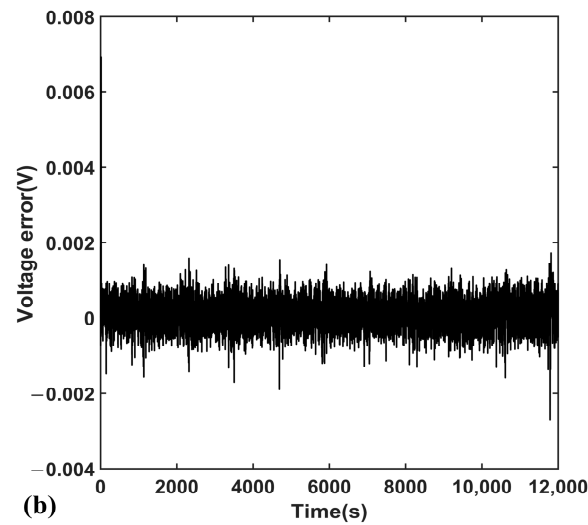


Figure 3. Result of terminal voltage prediction under New European Driving Cycle (NEDC) cycles: (a) Estimated terminal voltage versus measured data; (b) Estimated voltage error.

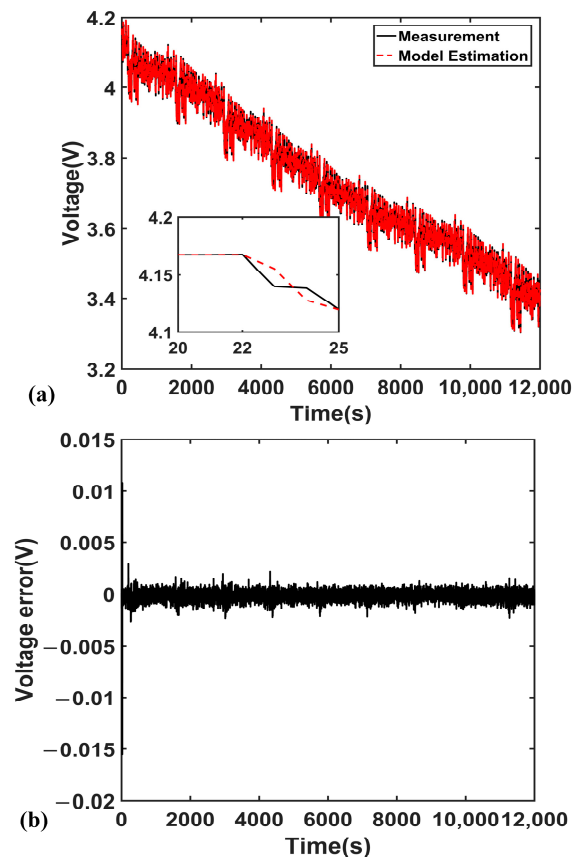


Figure 4. Result of terminal voltage prediction under Federal Urban Driving Schedule (FUDS) cycles: (a) Estimated terminal voltage versus measured data; (b) Estimated voltage error.

3. An Improved ACKF for SOC Estimation

It is well-known that both the process noise covariance and measurement noise covariance of KF-based algorithms have a distinct influence on their filtering performance and stability. In the standard CKF algorithm, both the process noise covariance and the measurement noise covariance are selected to be constant values, which need to be carefully pre-specified. Inappropriate values

of the process noise covariance or the measurement noise covariance or both usually cause a large estimation error. Furthermore, the values of these two noise covariances for a practical battery system in electric vehicles vary with random disturbances from sensor drift and parameter uncertainties due to battery time-varying behaviors. Therefore, adaptive update of the process noise covariance matrix and measurement noise covariance matrix could be helpful to improve aspects of the algorithm's performance, such as estimation accuracy and convergence rate. In this paper, an adaptive cubature Kalman filter based on the improved Sage–Husa maximum posterior estimator is proposed for battery SOC estimation. A recursive process based on the improved Sage–Husa maximum posterior estimator is employed to update the estimation of the unknown process noise covariance Q and measurement noise covariance R in each step. Then, the real-time updated noise statistical feature is substituted into the CKF algorithm, improving the filtering result of the CKF algorithm under unknown system noise.

The recursive process of the proposed adaptive cubature Kalman filter for battery SOC estimation can be summarized as follows [44]:

(1) Initialization of Parameters

- 1.1 Select the initial value of the posteriori error covariance P_0
- 1.2 Select the initial value of the process noise covariance Q_0
- 1.3 Select the initial value of the measurement noise covariance R_0
- 1.4 Calculate the initial mean value \bar{x}_0 and covariance P_0 with randomly selected state vector x_0 as follows:

$$\bar{x}_0 = E[x_0] \quad (15)$$

$$P_0 = E[(x_0 - \bar{x}_0)(x_0 - \bar{x}_0)^T]. \quad (16)$$

(2) Time update

- 2.1 Factorize the error covariance P_{k-1} as

$$S_{k-1} = chol(P_{k-1}) \quad (17)$$

where $chol(\cdot)$ represents the Cholesky decomposition.

- 2.2 Calculate the cubature points

$$x_{k-1}^{(i)} = S_{k-1}\zeta^{(i)} + \hat{x}_{k-1} \quad (18)$$

where $i = 1, 2, \dots, 2n$ (n denotes the number of state variables), and ζ is the set of standard cubature points given by:

$$\zeta^{(i)} = \begin{cases} \sqrt{n}[1]^{(i)} & i = 1, 2, \dots, n \\ -\sqrt{n}[1]^{(i)} & i = n + 1, n + 2, \dots, 2n \end{cases} \quad (19)$$

where $[1]^{(i)}$ represents the i -th column vector of identity matrix.

- 2.3 Propagate the cubature points through the process equation and calculate the predicted state values

$$\chi_k^{(i)} = f(x_{k-1}^{(i)}, u_{k-1}) \quad (20)$$

$$\bar{x}_k = \frac{1}{2n} \sum_{i=1}^{2n} \chi_k^{(i)}. \quad (21)$$

2.4 Calculate the propagated covariance

$$P_k = \frac{1}{2n} \sum_{i=1}^{2n} (\chi_k^{(i)} - \bar{x}_k)(\chi_k^{(i)} - \bar{x}_k)^T + Q_{k-1} \quad (22)$$

where Q_{k-1} denotes the process noise covariance matrix.

(3) Measurement update

3.1 Factorize the error covariance again

$$S_k = chol(P_k). \quad (23)$$

3.2 Recalculate the cubature points

$$x_k^{(i)} = S_k \xi^{(i)} + \hat{x}_k \quad (i = 1, 2, \dots, 2n). \quad (24)$$

3.3 Propagate the cubature points through the measurement equation and calculate the predicted measurement values

$$y_k^{(i)} = h(x_k^{(i)}, u_k) \quad (25)$$

$$\bar{y}_k = \frac{1}{2n} \sum_{i=1}^{2n} y_k^{(i)}. \quad (26)$$

3.4 Calculate the covariance estimation

$$P_k^y = \frac{1}{2n} \sum_{i=1}^{2n} (y_k^{(i)} - \bar{y}_k)(y_k^{(i)} - \bar{y}_k)^T + R_{k-1} \quad (27)$$

$$P_k^{xy} = \frac{1}{2n} \sum_{i=1}^{2n} (x_k^i - \bar{x}_k)(y_k^i - \bar{y}_k)^T \quad (28)$$

where R_{k-1} denotes the measurement noise covariance matrix.

3.5 Calculate the Kalman gain

$$K_k = P_k^{xy} (P_k^y)^{-1}. \quad (29)$$

3.6 Update the state prediction

$$\hat{x}_k = \bar{x}_k + K_k (y_k - \bar{y}_k) \quad (30)$$

where y_k represents the measured output, i.e., the battery terminal voltage for SOC estimation.

3.7 Update the error covariance

$$P_k = P_k - K_k P_k^y K_k^T. \quad (31)$$

(4) Adaptive update of Q_k and R_k .

As mentioned at the beginning of Section 3, the process noise covariance and measurement noise covariance are changeable due to random disturbances and parameter uncertainties. In this paper, according to the improved Sage–Husa maximum posterior estimator and the output voltage residual sequence of the battery model, both of these two noise covariance matrices are adaptively updated as:

$$\left. \begin{cases} d_k = \frac{1-b}{1-b^{k+1}} \\ F_k = e_k e_k^T \\ Q_k = (1-d_k)Q_{k-1} + d_k K F_k K^T \\ R_k = (1-d_k)R_{k-1} + d_k F_k \end{cases} \right\} \dots k < L; k = 1, 2, 3 \dots \quad (32)$$

$$\left. \begin{cases} Q_k = (1-d_k)Q_{k-1} + d_k (K F_k K^T + P_k - P_{k|k-1}) \\ R_k = (1-d_k)R_{k-1} + d_k (F_k - P_{k|k-1}^y) \end{cases} \right\} \dots k \geq L; k = L + N * S; N = 1, 2, 3 \dots$$

where b is a forgetting factor used to limit the memory length of the filter. Usually, the value of b is selected as $0.95 < b < 0.99$. A larger value of b means a stronger effect of newly measured data on the current estimation, so b should accordingly be a larger value when the noise statistics change rapidly. Herein, $b = 0.97$ is selected. e_k and F_k are the voltage residual and voltage residual squared error at time step k , respectively. L is a moment that changes a biased estimator to an unbiased estimator, and S is the step length. In this paper, $L = 1000$ and $S = 20$ are selected.

4. Experimental Verification and Discussion

4.1. Battery Test Bench

We established a test bench presented in Figure 5 to evaluate the proposed improved ACKF algorithm for battery SOC estimation. The test bench consists of a battery cycler, a desktop computer, and the tested lithium-ion battery.

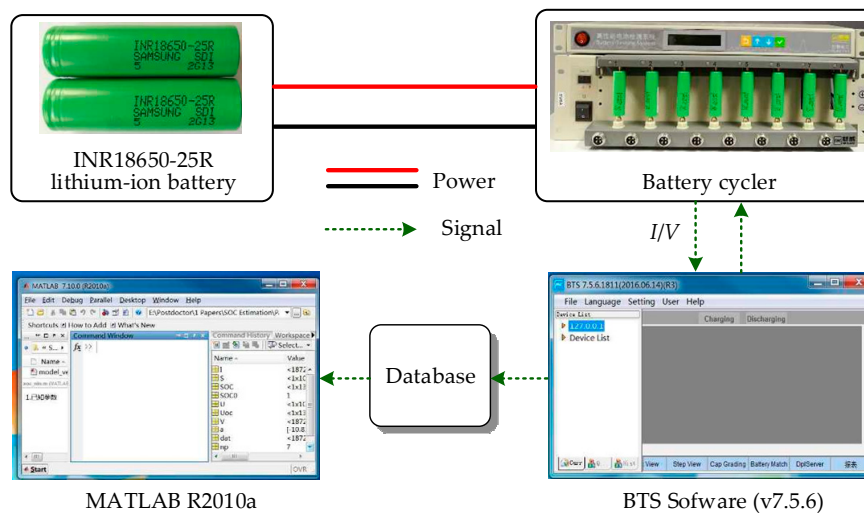


Figure 5. Configuration of the battery test bench.

The battery cycler specified as NEWARE BTS4000 is used to discharge and charge the battery cells according to the programmed current profiles, as well as to collect the battery voltage and current. The voltage and current measurement ranges of the cycler are 0~5 V and $-6\sim 6$ A, respectively, and the measurement accuracy of the voltage and current are both higher than 0.1%. The desktop computer is applied to control and monitor the battery cycler via Ethernet cables, as well as to store the voltage and current data collected by the battery cycler. The tested lithium-ion battery cells are INR18650-25R developed by SAMSUNG SDI, whose nominal capacity is 2500 mAh, nominal voltage is 3.6 V, charging and discharging cutoff voltages are 4.2 V and 2.5 V, respectively, and maximum continuous discharging current reaches to 20 A. The sampling period of the battery current and voltage are both selected to be one second. In this paper, we are concerned with the estimation accuracy and convergence rate at different initial SOC errors of the SOC estimation algorithms.

4.2. SOC Estimation Accuracy

Experimental data collected from typical driving cycle tests are commonly used to evaluate the properties of SOC estimation algorithms. In this section, the widely used New European Driving Cycle (NEDC) and Federal Urban Driving Schedule (FUDS) cycles are selected to simulate the typical driving conditions of electric vehicles on roads. Figures 6 and 7 respectively show the battery current profiles under the NEDC and FUDS cycles.

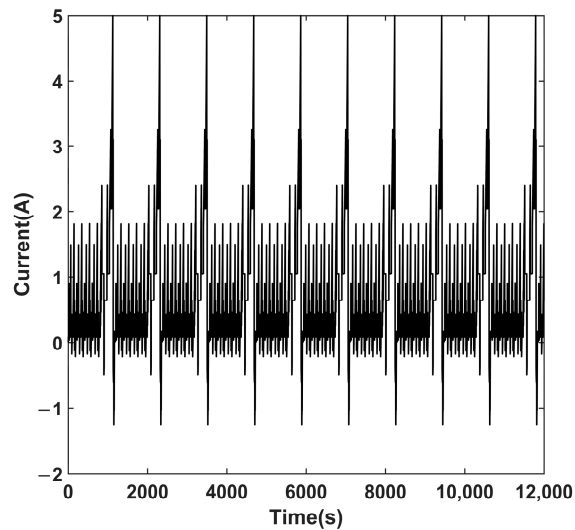


Figure 6. Current profile under the NEDC cycles.

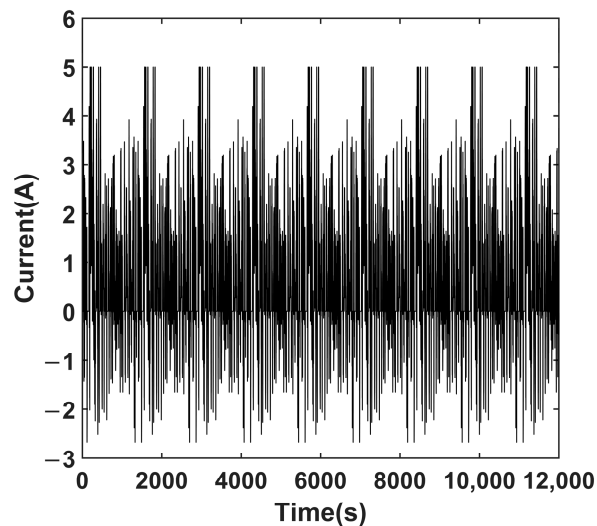


Figure 7. Current profile under the FUDS cycles.

The proposed ACKF algorithm was compared with two existing algorithms, i.e., the UKF and the standard CKF, to validate its effectiveness and superiority in improving SOC estimation accuracy. Specially, the online parameter identification is compared with the offline parameter identification to prove its benefit to accuracy improvement of SOC estimation.

The SOC estimation results under the NEDC and FUDS cycles are respectively shown in Figures 8 and 9, where the blue dashed-line represents the reference SOC calculated by the Coulomb counting methodology with accurately measured current values, the red solid-line reveals the estimated SOC using the UKF algorithm based on online parameter identification (FRLS-UKF), the green

solid-line indicates the estimated SOC using the traditional CKF algorithm based on online parameter identification (FRLS-CKF), the black solid-line describes the estimated SOC using the adaptive CKF algorithm based on online parameter identification (FRLS-ACKF), and the blue solid-line represents the estimated SOC using the ACKF algorithm based on offline parameter identification (offline-ACKF). The maximum error and root mean square error (RMSE) of the SOC estimation with precise initial SOC values are summarized in Table 1.

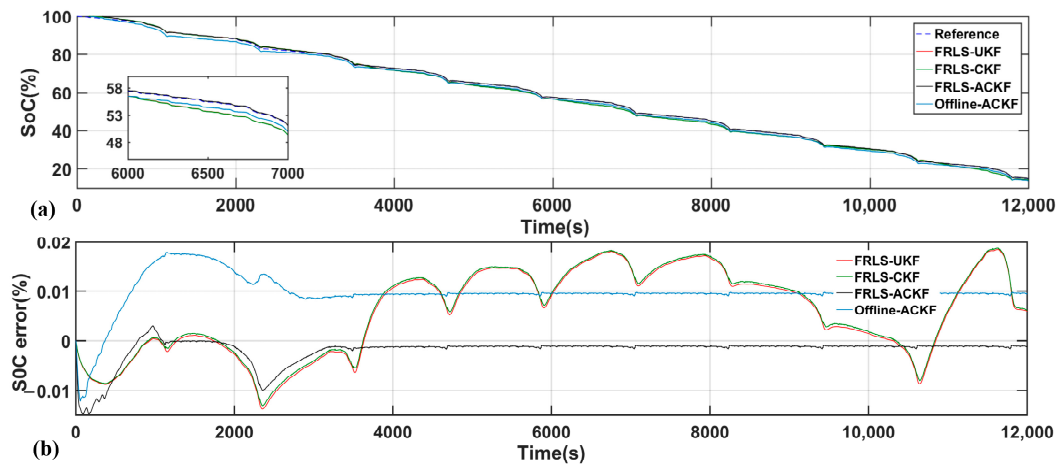


Figure 8. SOC estimation results without initial SOC error under NEDC cycles: (a) SOC; (b) SOC error. FRLS: forgetting factor recursive least squares; UKF: unscented Kalman filter; CKF: cubature Kalman filter; ACKF: adaptive cubature Kalman filter.

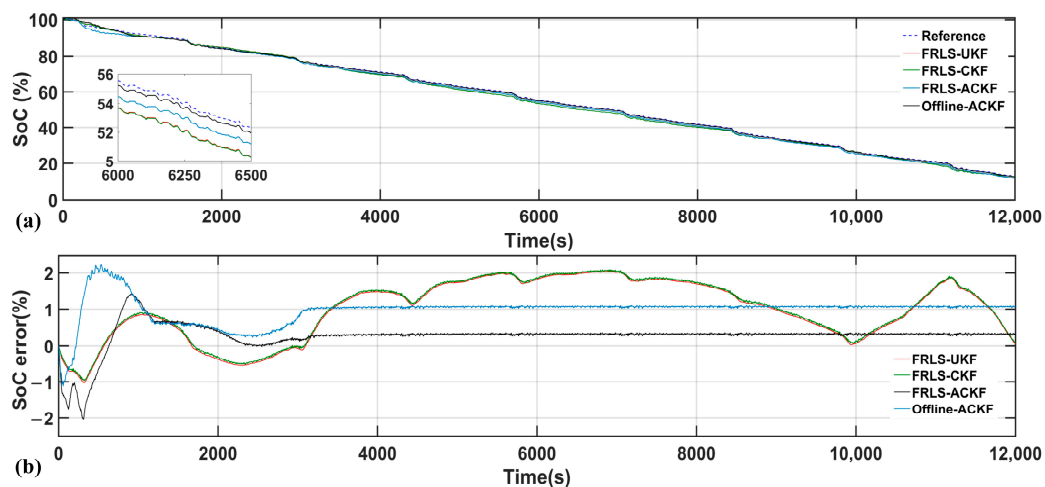


Figure 9. SOC estimation results without initial SOC error under FUDS cycles: (a) SOC; (b) SOC error.

Table 1. Comparison of SOC estimation without initial SOC error.

Methods	NEDC		FUDS	
	Maximum Error	RMSE	Maximum Error	RMSE
FRLS-UKF	1.84%	1.03%	2.04%	1.28%
FRLS-CKF	1.87%	1.05%	2.09%	1.30%
FRLS-ACKF	1.48%	0.32%	2.04%	0.47%
Offline-ACKF	1.79%	1.04%	2.22%	1.05%

RMSE: root mean square error.

It can be found from all of the above results that the proposed ACKF-based method is able to improve the SOC estimation accuracy under both the NEDC and FUDS cycles in comparison with the other three algorithms. For example, the SOC error is less than 1.48% and the RMSE is about 0.32% under the NEDC cycles. The maximum SOC error and RMSE are both smaller compared with the CKF and UKF algorithms under both the NEDC and FUDS cycles. Additionally, the proposed improved ACKF-based estimator can greatly reduce the SOC estimation fluctuation as compared with the UKF and CKF algorithms. Specially, the online parameter identification-based SOC estimation is more accurate and reliable compared with the offline parameter identification-based SOC estimation both using the ACKF, further validating the benefit of online parameter identification for the improvement of model accuracy and SOC estimation.

4.3. Convergence Ability with Initial SOC Error

Convergence rate is another important indicator for evaluating the SOC estimation algorithm. Herein, the steps converged to 5% error bound at different initial SOC values from 50% to 80% with 10% steps under the NEDC and FUDS cycles are obtained to assess the convergence behavior of the ACKF algorithm as compared with the CKF and UKF algorithms. Figure 10 presents the comparison results. It can be seen that the convergence rate of the ACKF algorithm is more than five times as fast as the other two algorithms. Taking as an example, Figure 11 shows the SOC estimation results of the four algorithms in Figures 8 and 9 with 70% initial SOC under the NEDC cycle. It is clear that the ACKF algorithm can quickly converge to the reference SOC values with different initial SOC errors compared with the UKF and CKF algorithms.

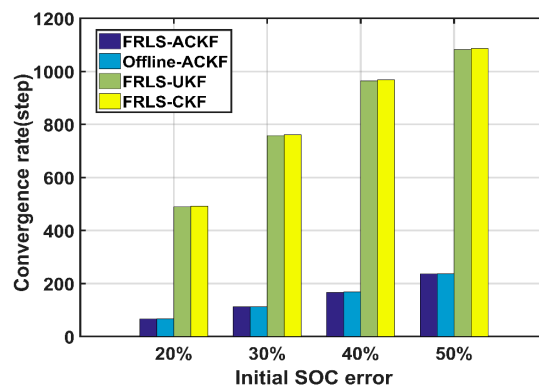


Figure 10. The convergence rate with different initial SOC errors.

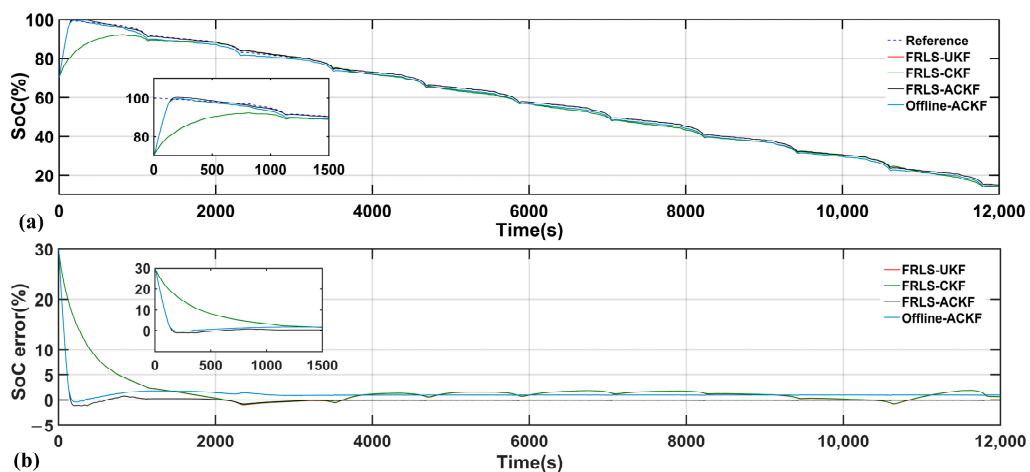


Figure 11. SOC estimation results with 30% initial SOC error under NEDC cycles: (a) SoC; (b) SoC error.

5. Conclusions

In this study, an improved ACKF-based battery SOC estimation algorithm has been proposed. Since battery model accuracy has a remarkable influence on SOC estimation, parameters of the Thevenin battery equivalent circuit model are updated online using the forgetting factor recursive least squares (FRLS) algorithm. Experiments based on the NEDC and FUDS cycles are performed to evaluate the effectiveness and superiority of the proposed method as compared with two existing SOC estimation algorithms, including the UKF and the standard CKF, in terms of estimation accuracy and convergence rate. Comparison results reveal that the presented improved ACKF-based estimator can rapidly converge to the reference SOC values at different initial SOC errors. Exactly, its convergence rate is more than five times as fast as the other two algorithms. In addition, it has a higher tracking accuracy with lower fluctuation. Furthermore, online parameter identification-based SOC estimation is highly beneficial to further accuracy improvement. The converged RMSE of SOC estimation without initial SOC error is less than 0.5% under the NEDC and FUDS cycles.

Acknowledgments: This work was simultaneously supported by the Natural Science Foundation of Guangdong Province (No. 2016A030313056, No. 2017A030310011), the Science and Technology Plan Project of Shenzhen (No. JCYJ20160308092940394, No. JCYJ20170412110241478), and the Natural Science Foundation of Shenzhen University (No. 2016027).

Author Contributions: Zhibing Zeng and Yong Tian presented the original idea of the research and prepared the manuscript. Zhibing Zeng, Dong Li, and Yong Tian performed the experiments together. The final manuscript was corrected by Jindong Tian and Yong Tian.

Conflicts of Interest: The authors declare no conflict of interest.

References

1. Safari, M.; Morcrette, M.; Teyssot, A.; Delacourt, C. Life-prediction methods for lithium-ion batteries derived from a fatigue approach I. introduction: Capacity-loss prediction based on damage accumulation. *J. Electrochem. Soc.* **2010**, *157*, A713–A720. [[CrossRef](#)]
2. Bucci, G.; Swamy, T.; Chiang, Y.-M.; Carter, W.C. Modeling of internal mechanical failure of all-solid-state batteries during electrochemical cycling, and implications for battery design. *J. Mater. Chem. A* **2017**, *5*, 19422–19430. [[CrossRef](#)]
3. Waag, W.; Käbitz, S.; Sauer, D.U. Experimental investigation of the lithium-ion battery impedance characteristic at various conditions and aging states and its influence on the application. *Appl. Energy* **2013**, *102*, 885–897. [[CrossRef](#)]
4. Cheng, X.-B.; Zhang, R.; Zhao, C.-Z.; Wei, F.; Zhang, J.-G.; Zhang, Q. A Review of solid electrolyte interphases on lithium metal anode. *Adv. Sci.* **2016**, *3*, 2198–3844. [[CrossRef](#)] [[PubMed](#)]
5. Peabody, C.; Arnold, C.B. The role of mechanically induced separator creep in lithium-ion battery capacity fade. *J. Power Sources* **2011**, *196*, 8147–8153. [[CrossRef](#)]
6. Behrou, R.; Maute, K. Numerical modeling of damage evolution phenomenon in solid-state lithium-ion batteries. *J. Electrochem. Soc.* **2017**, *164*, A2573–A2589. [[CrossRef](#)]
7. Behrou, R.; Maute, K. Multiscale modeling of non-local damage evolution in lithium-ion batteries. *ECS Trans.* **2017**, *77*, 1163–1179. [[CrossRef](#)]
8. Xing, Y.; Ma, E.W.; Tsui, K.L.; Pecht, M. Battery management systems in electric and hybrid vehicles. *Energies* **2011**, *4*, 1840–1857. [[CrossRef](#)]
9. Fleischer, C.; Waag, W.; Heyn, H.; Sauer, D. On-line adaptive battery impedance parameter and state estimation considering physical principles in reduced order equivalent circuit battery models Part 1. Requirements, critical review of methods and modeling. *J. Power Sources* **2014**, *260*, 276–291. [[CrossRef](#)]
10. Wang, Y.; Zhang, C.; Chen, Z. A method for state-of-charge estimation of Li-ion batteries based on multi-model switching strategy. *Appl. Energy* **2015**, *137*, 427–434. [[CrossRef](#)]
11. Soon, K.; Moo, C.; Chen, Y.; Hsieh, Y. Enhanced coulomb counting method for estimating state-of-charge and state-of-health of lithium-ion batteries. *Appl. Energy* **2009**, *86*, 1506–1511.
12. Yang, N.; Zhang, X.; Li, G. State of charge estimation for pulse discharge of a LiFePO₄ battery by a revised Ah counting. *Electrochim. Acta* **2015**, *151*, 63–71. [[CrossRef](#)]

13. Lee, S.; Kim, J.; Lee, J.; Cho, B.H. State-of-charge and capacity estimation of lithium-ion battery using a new open-circuit voltage versus state-of-charge. *J. Power Sources* **2008**, *185*, 1367–1373. [[CrossRef](#)]
14. Dubarry, M.; Svoboda, V.; Hwu, R.; Liaw, B. Capacity loss in rechargeable lithium cells during cycle life testing: The importance of determining state-of-charge. *J. Power Sources* **2007**, *174*, 1121–1125. [[CrossRef](#)]
15. Dang, X.; Yan, L.; Xu, K.; Wu, X.; Jiang, H.; Sun, H. Open-circuit voltage-based state of charge estimation of lithium-ion battery using dual neural network fusion battery model. *Electrochim. Acta* **2016**, *188*, 356–366. [[CrossRef](#)]
16. Guo, Y.F.; Zhao, Z.S.; Huang, L.M. SOC Estimation of lithium battery based on improved BP neural network. *Energy Procedia* **2017**, *105*, 4153–4158. [[CrossRef](#)]
17. Anton, J.C.A.; Nieto, P.J.G.; Viejo, C.B.; Vilán, J.A.V. Support vector machines used to estimate the battery state of charge. *IEEE Trans. Power Electron.* **2013**, *28*, 5919–5926. [[CrossRef](#)]
18. Andre, D.; Appel, C.; Soczka-Guth, T.; Sauer, D.U. Advanced mathematical methods of SOC and SOH estimation for lithium-ion batteries. *J. Power Sources* **2013**, *224*, 20–27. [[CrossRef](#)]
19. Li, I.; Wang, W.Y.; Su, S.F.; Lee, Y.S. A merged fuzzy neural network and its applications in battery state-of-charge estimation. *IEEE Trans. Energy Convers.* **2007**, *22*, 697–708. [[CrossRef](#)]
20. Plett, G.L. Extended Kalman filtering for battery management systems of LiPB-based HEV battery packs Part 3. State and parameter estimation. *J. Power Sources* **2004**, *134*, 277–292. [[CrossRef](#)]
21. Lee, J.; Nam, O.; Cho, B.H. Li-ion battery SOC estimation method based on the reduced order extended Kalman filtering. *J. Power Sources* **2007**, *174*, 9–15. [[CrossRef](#)]
22. Han, J.Y.; Kim, D.C.; Sunwoo, M. State-of-charge estimation of lead-acid batteries using an adaptive extended Kalman filter. *J. Power Sources* **2009**, *188*, 606–612. [[CrossRef](#)]
23. Sun, F.C.; Hu, X.S.; Zou, Y.; Li, S.G. Adaptive unscented Kalman filtering for state of charge estimation of a lithium-ion battery for electric vehicles. *Energy* **2011**, *36*, 3531–3540. [[CrossRef](#)]
24. Zhang, C.P.; Jiang, J.C.; Zhang, W.G.; Sharkh, S.M. Estimation of state of charge of lithium-ion batteries used in HEV using robust extended Kalman filtering. *Energies* **2012**, *5*, 1098–1115. [[CrossRef](#)]
25. Hu, C.; Youn, B.D.; Chung, J. A multiscale framework with extended Kalman filter for lithium-ion battery SOC and capacity estimation. *Appl. Energy* **2012**, *92*, 694–704. [[CrossRef](#)]
26. Yuan, S.F.; Wu, H.J.; Yin, C.L. State of charge estimation using the extended Kalman filter for battery management systems based on the ARX battery model. *Energies* **2013**, *6*, 444–470. [[CrossRef](#)]
27. Chen, Z.; Fu, Y.H.; Mi, C.C. State of charge estimation of lithium-ion batteries in electric drive vehicles using extended Kalman filtering. *IEEE Trans. Veh. Technol.* **2013**, *62*, 1020–1030. [[CrossRef](#)]
28. Sepasi, S.; Ghorbani, R.; Liaw, B.Y. A novel on-board state-of-charge estimation method for aged Li-ion batteries based on model adaptive extended Kalman filter. *J. Power Sources* **2014**, *245*, 337–344. [[CrossRef](#)]
29. Bizeray, A.M.; Zhao, S.; Duncan, S.R.; Howey, D.A. Lithium-ion battery thermal-electrochemical model-based state estimation using orthogonal collocation and a modified extended Kalman filter. *J. Power Sources* **2015**, *296*, 400–412. [[CrossRef](#)]
30. Pérez, G.; Garmendia, M.; Reynaud, J.F.; Crego, J.; Viscarret, U. Enhanced closed loop State of Charge estimator for lithium-ion batteries based on Extended Kalman Filter. *Appl. Energy* **2015**, *155*, 834–845. [[CrossRef](#)]
31. Pavković, D.; Krznar, M.; Komljenović, A.; Hrgetić, M.; Zorc, D. Dual EKF-Based State and Parameter Estimator for a LiFePO₄ Battery Cell. *J. Power Electron.* **2017**, *17*, 398–410. [[CrossRef](#)]
32. Pan, H.H.; Lu, Z.Q.; Lin, W.L.; Li, J.Z.; Chen, L. State of charge estimation of lithium-ion batteries using a grey extended Kalman filter and a novel open-circuit voltage model. *Energy* **2017**, *138*, 764–775. [[CrossRef](#)]
33. Plett, G.L. Sigma-point Kalman filtering for battery management systems of LiPB-based HEV battery packs-Part 1: Introduction and state estimation, Part 2: Simultaneous state and parameter estimation. *J. Power Sources* **2006**, *161*, 1369–1384. [[CrossRef](#)]
34. He, Z.W.; Gao, M.Y.; Wang, C.S.; Wang, L.Y.; Liu, Y.Y. Adaptive state of charge estimation for Li-ion batteries based on an unscented Kalman filter with an enhanced battery model. *Energies* **2013**, *6*, 4134–4151. [[CrossRef](#)]
35. Tian, Y.; Xia, B.Z.; Sun, W.; Xu, Z.H.; Zheng, W.W. A modified model based state of charge estimation of power lithium-ion batteries using unscented Kalman filter. *J. Power Sources* **2014**, *270*, 619–626. [[CrossRef](#)]
36. Htet, A.; Kay, S.L.; Shu, T.G. State-of-charge estimation of lithium-ion battery using square root spherical unscented Kalman filter (Sqrt-UKFST) in nanosatellite. *IEEE Trans. Power Electron.* **2015**, *30*, 4774–4783.

37. Meng, J.H.; Luo, G.Z.; Gao, F. Lithium polymer battery state-of-charge estimation based on adaptive unscented Kalman filter and support vector machine. *IEEE Trans. Power Electron.* **2016**, *31*, 2226–2238. [[CrossRef](#)]
38. He, H.W.; Xiong, R.; Peng, J.K. Real-time estimation of battery state-of-charge with unscented Kalman filter and RTOS μ COS-II platform. *Appl. Energy* **2016**, *162*, 1410–1418. [[CrossRef](#)]
39. Peng, S.; Chen, C.; Shi, H.B.; Yao, Z.L. State of charge estimation of battery energy storage systems based on adaptive unscented Kalman filter with a noise statistics estimator. *IEEE Access* **2017**, *5*, 13202–13212. [[CrossRef](#)]
40. Yu, Q.Q.; Xiong, R.; Lin, C.; Shen, W.X.; Deng, J.J. Lithium-Ion Battery Parameters and State-of-Charge Joint Estimation Based on H-Infinity and Unscented Kalman Filters. *IEEE Trans. Veh. Technol.* **2017**, *66*, 8693–8701. [[CrossRef](#)]
41. Li, J.H.; Barillas, J.K.; Guenther, C.; Danzer, M.A. A comparative study of state of charge estimation algorithms for LiFePO₄ batteries used in electric vehicles. *J. Power Sources* **2013**, *230*, 244–250. [[CrossRef](#)]
42. Arasaratnam, I.; Haykin, S. Cubature Kalman filters. *IEEE Trans. Autom. Control* **2009**, *54*, 1254–1269. [[CrossRef](#)]
43. Arasaratnam, I.; Haykin, S.; Hurd, T.R. Cubature Kalman filtering for continuous-discrete systems: Theory and simulations. *IEEE Trans. Signal Process.* **2010**, *58*, 4977–4993. [[CrossRef](#)]
44. Xia, B.; Wang, H.; Tian, Y.; Wang, M.; Sun, W.; Xu, Z. State of charge estimation of lithium-ion batteries using an adaptive cubature Kalman filter. *Energies* **2015**, *8*, 5916–5936. [[CrossRef](#)]



© 2018 by the authors. Licensee MDPI, Basel, Switzerland. This article is an open access article distributed under the terms and conditions of the Creative Commons Attribution (CC BY) license (<http://creativecommons.org/licenses/by/4.0/>).